

PHASEMARK: A POST-HOC, OPTIMIZATION-FREE WATERMARKING OF AI-GENERATED IMAGES IN THE LATENT FREQUENCY DOMAIN

Sung Ju Lee Nam Ik Cho

Department of ECE & INMC, Seoul National University, Korea

ABSTRACT

The proliferation of hyper-realistic images from Latent Diffusion Models (LDMs) demands robust watermarking, yet existing post-hoc methods are prohibitively slow due to iterative optimization or inversion processes. We introduce PhaseMark, a single-shot, optimization-free framework that directly modulates the phase in the VAE latent frequency domain. This approach makes PhaseMark thousands of times faster than optimization-based techniques while achieving state-of-the-art resilience against severe attacks, including regeneration, without degrading image quality. We analyze four modulation variants, revealing a clear performance-quality trade-off. PhaseMark demonstrates a new paradigm where efficient, resilient watermarking is achieved by exploiting intrinsic latent properties.

Index Terms— Latent Phase, Watermarking, LDMs

1. INTRODUCTION

Recent advances in Latent Diffusion Models (LDMs) [1] enable hyper-realistic image generation, necessitating robust watermarking for copyright protection and content authentication. However, traditional frequency-based methods [2, 3] are vulnerable to modern threats like regeneration attacks, requiring a new paradigm for the generative AI era.

Recent post-hoc latent space watermarking methods show resilience to regeneration attacks but suffer from prohibitive computational costs. For instance, ZoDiac [4] and FreqMark [5] rely on a multi-minute, per-image optimization process; other prominent methods employ DDIM inversion [4, 6, 7, 8, 9], which requires multiple expensive LDM executions for detection. This high computational barrier impedes real-world deployment.

We propose PhaseMark, a single-shot, optimization-free post-hoc watermarking framework that overcomes these limitations. PhaseMark directly modulates the phase in the mid-band frequency of the VAE latent vector. Our contributions are: First, PhaseMark is thousands of times faster than optimization-based methods while achieving comparable or superior resilience to regeneration attacks. Second, we design and analyze four variants along the axes of *absolute*

vs. *relative phase* and *hard* vs. *soft* modulation, revealing a clear trade-off between performance and image quality. We demonstrate that expensive optimization is not a prerequisite for resilience; rather, it is achievable by efficiently exploiting the latent space’s intrinsic properties.

2. LATENT PHASE WATERMARKING

PhaseMark is a fast, robust, post-hoc watermarking model that directly modulates the phase in a VAE’s latent frequency domain in a single-shot, achieving high efficiency and robustness without iterative optimization.

2.1. Overall Framework

The VAE encoder first maps an input image \mathcal{I} to a latent vector z_0 . For spatial robustness, we apply a 2D FFT to its central region, z_{crop} , yielding $\mathcal{F}(z_{crop})$. An L -bit message M is embedded into L 2×2 blocks, $\mathcal{B} = \{B_1, \dots, B_L\}$, extracted from stable mid-band frequencies. This selection avoids low-frequency image content and high-frequency noise. Block selection uses axis offsets to bypass principal axes. After modulation, Hermitian symmetry is enforced to ensure a real-valued output after the Inverse FFT. Finally, the VAE decoder reconstructs the watermarked image \mathcal{I}' .

2.2. Phase Modulation for Embedding

To embed a message bit m_i into each extracted block B_i , we propose four phase modulation strategies, which are categorized into two distinct families.

2.2.1. Absolute Phase Modulation

Methods in this family modulate the phase of complex numbers within a block to predefined absolute values, which are independent of other elements.

Absolute Phase Modulation (APM). APM, a *hard* modulation method, forcibly assigns the phase of each complex number c in block B_i based on the message bit m_i :

$$\angle c' = (-1)^{1-m_i} \frac{\pi}{2} \quad (1)$$

Phase Constellation Quantization (PCQ). This *soft* modulation method is designed to minimize image distortion. Two phase constellation sets \mathcal{P}_0 and \mathcal{P}_1 are predefined based on the bit value. The original phase $\angle c$ of each complex number c within block B_i is then quantized to the nearest phase in the constellation set corresponding to the bit:

$$\angle c' = \arg \min_{p \in \mathcal{P}_{m_i}} |\angle c - p|_{\text{angle}} \quad (2)$$

Here, $|\cdot|_{\text{angle}}$ denotes the minimum angular distance.

2.2.2. Relative Phase Modulation

This family of methods encodes information in the relative phase relationships among elements within a block. For a 2×2 block $B_i = \{c_1, c_2, c_3, c_4\}$ the elements c_1 and c_3 serve as anchors.

Intra-block Phase Synchronization (IPS). A *hard* relative modulation method that forcibly synchronizes the phases of c_2 and c_4 with those of the anchors c_1 and c_3 , while preserving their original magnitudes.

$$\begin{aligned} \angle c'_2 &\leftarrow \angle c_1 + (1 - m_i)\pi \\ \angle c'_4 &\leftarrow \angle c_3 + (1 - m_i)\pi \end{aligned} \quad (3)$$

Soft Phase Synchronization (SPS). SPS, a *soft* method, interpolates vectors c_2 and c_4 towards their phase-synchronized targets. The modified vector c'_k for $k \in \{2, 4\}$ is a linear interpolation between the original c_k and its target $c_{k,\text{tgt.}}$:

$$c'_k = (1 - \gamma)c_k + \gamma \cdot c_{k,\text{tgt.}} \quad \text{for } k \in \{2, 4\}, \quad (4)$$

where $c_{k,\text{tgt.}} = |c_k|e^{j\phi_{k,\text{tgt.}}}$ and $\phi_{k,\text{tgt.}} = \angle c_{k-1} + (1 - m_i)\pi$. Here, $\gamma \in [0, 1]$ is an interpolation strength parameter. Note that when $\gamma = 1$, SPS becomes identical to IPS.

2.3. Watermark Detection

Detection reverses the embedding process to extract blocks \mathcal{B}' and message \hat{m} . The bit \hat{m}_i from each block B'_i is determined as follows:

APM. The sign of the sum of all phases within the block determines the bit. If $\sum_{c \in B'_i} \angle c > 0$, then $\hat{m}_i = 1$; otherwise, $\hat{m}_i = 0$.

PCQ. The bit is determined by comparing the total distance from the block's phases to each of the two constellation sets, \mathcal{P}_0 and \mathcal{P}_1 .

IPS & SPS. A correlation score which represents the phase relationship with the anchor points is calculated: $S_i = \cos(\angle c_1 - \angle c_2) + \cos(\angle c_3 - \angle c_4)$. If $S_i > 0$, then $\hat{m}_i = 1$; otherwise, $\hat{m}_i = 0$.

A watermark is detected if the Bit Accuracy (BA) exceeds a threshold τ set for a 1% False Positive Rate (FPR). The verification ($\tau_{\text{vrf.}}$) and identification ($\tau_{\text{idf.}}$) thresholds are defined as: $\tau_{\text{vrf.}} = \frac{1}{L} \min\{k \mid P(\text{matches} \geq k) \leq \alpha\}$. For identification among $N = 10^6$ users, a more stringent threshold

is derived using a Bonferroni correction: $\tau_{\text{idf.}} = \frac{1}{L} \min\{k \mid P(\text{matches} \geq k) \leq \alpha/N\}$. The performance for both tasks is evaluated as the True Positive Rate (TPR) at the prespecified 1% FPR.

3. EXPERIMENTS

3.1. Experimental Setup and Implementation Details

Datasets & Generation. We generate 1,000 512×512 images per dataset using Stable Diffusion v2-1-base model [1] ($\text{CFG} = 7.5$, 50 DDIM steps). Prompts are from MS-COCO-2017 [10], with SD-Prompts [11] and DiffusionDB [12] for generalization.

Watermarking Setup. We use the LDM's VAE. Latent crop z_{crop} is $44 \times 44 \times 4$, mid-band frequencies are radially bounded by [10, 18], and the message is 32 bits per channel. We set $\gamma = 0.8$ for SPS.

Baselines. We compare against post-hoc (DwtDctSvd [2], RivaGAN [13], ZoDiac [4]) and in-generation (S.Sign. [14], Tree-Ring [6], RingID [7], G.Shading [8], SFW [9]) methods.

Attacks. We evaluate robustness against nine attacks: contrast (0.5), JPEG ($Q = 25$), Gaussian blur ($r = 5$), BM3D ($\sigma = 0.1$), VAE regeneration (VAE-B [15] and VAE-C [16]) with a quality level of 3), diffusion regeneration [17] (60 steps), and center/random crops (0.5/0.7 scale).

Metrics. Detection performance is measured by TPR@1%FPR. FID score [18] is calculated between the 1,000 watermarked images and corresponding images from the MS-COCO. (FID-1k)

3.2. Comparison with Baselines

This section presents a quantitative comparison of our proposed watermarking methodology against state-of-the-art techniques, evaluating resilience, image quality, and computational efficiency.

Resilience and Image Quality. As shown in Table 1, our performance-centric model (Ours-Perf., APM) achieves a 0.999 verification rate, comparable to leading in-generation methods like SFW and G.Shading. Notably, it achieves this single-shot resilience to regeneration attacks post-hoc, a capability previously considered exclusive to in-generation techniques. Its center-aware design also provides significant defense against cropping attacks, with a success rate approaching 1.0. Image quality is evaluated using the FID score to ensure a fair comparison with in-generation techniques, which lack reference images. The $\Delta\text{FID-1k}$ values in Table 1 show that our methodology causes almost no degradation in image quality. Our quality-centric model, Ours-Qual. (PCQ), even slightly improves image quality, with a $\Delta\text{FID-1k}$ of -0.517. The APM variant shows only a negligible change of +0.042. This performance represents a clear advantage over recent methods such as Tree-Ring (+1.184) and RingID (+2.054), which incur significant quality degradation.

Table 1. Comparison of detection performance (TPR@1%FPR) and image quality (Δ FID-1k) against baseline methods under various attacks. Ours-Perf (APM) and Ours-Qual (PCQ) denote our performance- and quality-centric models, respectively.

| Verification Task | Methods | Post-hoc | Bits | Signal Processing Attacks | | | | Regeneration Attacks | | | Cropping Attacks | | | Quality |
|---------------------|------------------|----------|----------|---------------------------|-------|-------|-------|----------------------|-------|-------|------------------|-------|-------|---------|
| | | | | Clean | Cont. | JPEG | Blur | BM3D | VAE-B | VAE-C | Diff. | C.C. | R.C. | |
| | DwtDctSvd | ✓ | 32 | 1.000 | 0.106 | 0.173 | 1.000 | 0.609 | 0.205 | 0.060 | 0.555 | 1.000 | 0.229 | 0.494 |
| | RivaGAN | ✓ | 32 | 1.000 | 0.997 | 0.798 | 1.000 | 0.972 | 0.025 | 0.016 | 0.998 | 0.998 | 0.119 | 0.692 |
| | S.Sign. | ✗ | 48 | 1.000 | 0.993 | 0.927 | 0.990 | 0.933 | 0.677 | 0.667 | 0.997 | 0.999 | 0.003 | 0.819 |
| | G.Shading | ✗ | 256 | 1.000 | 1.000 | 1.000 | 1.000 | 1.000 | 0.996 | 1.000 | 1.000 | 1.000 | 1.000 | -0.317 |
| | Tree-Ring | ✗ | zero-bit | 0.957 | 0.900 | 0.548 | 0.934 | 0.815 | 0.509 | 0.536 | 0.543 | 0.509 | 0.734 | 0.699 |
| | RingID | ✗ | zero-bit | 1.000 | 1.000 | 1.000 | 1.000 | 1.000 | 0.992 | 1.000 | 1.000 | 1.000 | 1.000 | 2.054 |
| | ZoDiac | ✓ | zero-bit | 0.998 | 0.998 | 0.973 | 0.998 | 0.997 | 0.944 | 0.958 | 0.972 | 0.989 | 0.995 | 0.982 |
| | SFW-HSQR | ✗ | zero-bit | 1.000 | 1.000 | 1.000 | 1.000 | 1.000 | 0.992 | 1.000 | 1.000 | 1.000 | 1.000 | -0.721 |
| | Ours-Qual. (PCQ) | ✓ | 128 | 1.000 | 0.988 | 0.870 | 0.998 | 0.992 | 0.918 | 0.933 | 1.000 | 0.999 | 0.998 | 0.970 |
| | Ours-Perf. (APM) | ✓ | 128 | 1.000 | 1.000 | 1.000 | 1.000 | 1.000 | 0.996 | 0.997 | 1.000 | 1.000 | 1.000 | 0.999 |
| Identification Task | Methods | Post-hoc | User IDs | Clean | Cont. | JPEG | Blur | BM3D | VAE-B | VAE-C | Diff. | C.C. | R.C. | Avg |
| | DwtDctSvd | ✓ | 10^6 | 1.000 | 0.019 | 0.000 | 0.999 | 0.037 | 0.000 | 0.000 | 0.000 | 0.000 | 0.003 | 0.206 |
| | RivaGAN | ✓ | 10^6 | 0.974 | 0.772 | 0.023 | 0.961 | 0.348 | 0.000 | 0.000 | 0.852 | 0.909 | 0.000 | 0.484 |
| | S.Sign. | ✗ | 10^6 | 0.989 | 0.948 | 0.067 | 0.632 | 0.285 | 0.008 | 0.008 | 0.970 | 0.982 | 0.000 | 0.489 |
| | G.Shading | ✗ | 10^6 | 1.000 | 1.000 | 0.999 | 1.000 | 1.000 | 0.992 | 0.999 | 1.000 | 1.000 | 1.000 | 0.999 |
| | Tree-Ring | ✗ | 2048 | 0.303 | 0.207 | 0.072 | 0.256 | 0.162 | 0.083 | 0.072 | 0.054 | 0.009 | 0.033 | 0.125 |
| | RingID | ✗ | 2048 | 1.000 | 1.000 | 0.975 | 1.000 | 0.996 | 0.978 | 0.970 | 0.998 | 0.874 | 0.978 | 0.977 |
| | ZoDiac | ✓ | 64 | 0.164 | 0.038 | 0.000 | 0.080 | 0.027 | 0.001 | 0.002 | 0.000 | 0.000 | 0.000 | 0.031 |
| | SFW-HSQR | ✗ | 8192 | 1.000 | 1.000 | 0.990 | 1.000 | 0.999 | 0.976 | 0.982 | 1.000 | 1.000 | 0.999 | 0.995 |
| | Ours-Qual. (PCQ) | ✓ | 10^6 | 1.000 | 0.848 | 0.427 | 0.972 | 0.849 | 0.573 | 0.592 | 0.933 | 0.981 | 0.989 | 0.816 |
| | Ours-Perf. (APM) | ✓ | 10^6 | 1.000 | 1.000 | 0.984 | 1.000 | 0.999 | 0.945 | 0.954 | 1.000 | 1.000 | 1.000 | 0.988 |

Table 2. Computational efficiency comparison. PhaseMark’s embedding and detection times are orders of magnitude faster than ZoDiac, enabling real-time processing.

| Methods | Approach | Opt.Free | Train Cost | Latency- \mathcal{E} | Latency- \mathcal{D} |
|-----------------|---------------------------------------|----------|------------------|------------------------|------------------------|
| RivaGAN | End-to-end Training | ✗ | 300 epochs | 0.416 s | 0.399 s |
| S.Sign. | End-to-end Training | ✗ | ≥ 50 epochs | - | 0.101 s |
| ZoDiac | Iterative Optimization | ✗ | 100 iters/img | 7.334 m | 4.113 s |
| <i>Semantic</i> | Iterative Inversion (\mathcal{D}) | ✓ | - | - | - |
| Ours | Single-Shot Transform | ✓ | - | 0.142 s | 0.050 s |

Computational Efficiency. Table 2 compares the computational efficiency of each methodology. End-to-end learning methods require substantial training costs in addition to their inference time. ZoDiac, our most direct comparison, is also a post-hoc latent space method, yet it requires over seven minutes for embedding (\mathcal{E}) a single image due to iterative optimization. Semantic-in-generation methods (*Semantic*) require a costly DDIM inversion process for detection (\mathcal{D}), averaging four seconds and demanding significant GPU resources per image. In contrast, our method uses only a single, lightweight VAE model, enabling real-time processing for both embedding (\mathcal{E} , 0.142s) and detection (\mathcal{D} , 0.050s). This demonstrates that high resilience and quality can be achieved simultaneously without heavy computational cost.

3.3. Analysis of Proposed Variants

This section analyzes the performance of the four proposed watermarking variants and validates the effect of a key design

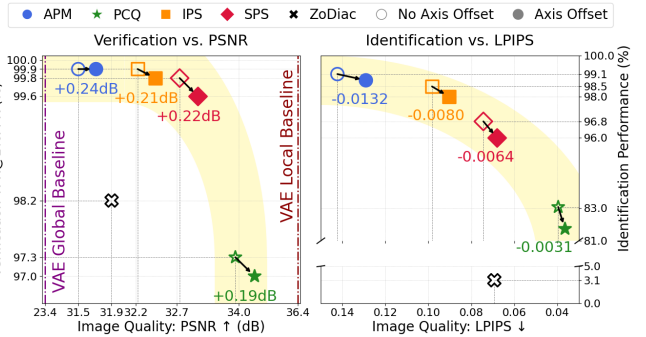


Fig. 1. Performance vs. image quality trade-off for the four proposed variants (APM, PCQ, IPS, SPS). The comparison includes ZoDiac and illustrates the positive effect of applying axis offsets.

component, the *Axis Offset*.

Trade-off between Detection and Quality. Figure 1 illustrates the performance-quality relationship of the four proposed variants and compares them with ZoDiac. The left plot shows verification performance versus PSNR, while the right plot shows identification performance versus LPIPS [19]. The four proposed variants form a distinct trade-off between detection performance and image quality, highlighted by the yellow shaded region in the figure. This trade-off allows users to select an optimal model based on their requirements, ranging from the performance-centric APM to the quality-centric PCQ. In terms of image quality, our quality-centric variant (PCQ with axis offsets) achieves a PSNR of 34.156. This

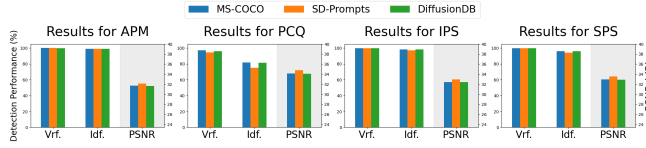


Fig. 2. Generalization performance. PhaseMark maintains consistent detection rates and image quality across three datasets, demonstrating high stability.

value is only marginally lower than the VAE’s maximum reconstruction fidelity of 36.4193 on our dataset and is substantially higher than the established VAE performance baseline of 23.4 ± 3.8 on the official benchmark. This demonstrates that the proposed method preserves high fidelity, especially considering the inherent information loss of the underlying VAE. ZoDiac is included for comparison because it is the only publicly available technique that can embed a watermark into the latent domain as a post-hoc process. ZoDiac performs adequately in the verification task, but its performance collapses to 3.1% in the identification task, rendering it unusable. This stands in stark contrast to our proposed variants, all of which exhibit strong performance on both tasks.

Axis offsets. All of our final proposed models apply the *Axis Offset* technique. To verify its effect, Figure 1 plots each variant with and without the axis offset applied. As the arrows in Figure 1 indicate, applying the axis offset improves image quality (higher PSNR, lower LPIPS) at the cost of a minor drop in detection performance. This is because it avoids modulating high-energy principal frequency axes, minimizing quality degradation. Given the substantial quality gain for a small performance trade-off, we incorporate it into all final models. This tendency is consistently observed in the results of the subsequent ablation study (Table 3).

Generalization Performance. To verify the generalization performance of our methodology, we evaluate it on two additional datasets: SD-Prompts [11] and DiffusionDB [12]. The results presented in Figure 2 show that the proposed methods exhibit consistent detection performance and image quality across these diverse datasets, demonstrating high stability.

3.4. Ablation Study

This section presents the results of an ablation study on the key parameters of our methodology. For brevity, we summarize the results for IPS, the variant with the most balanced performance, as a representative case in Table 3. All other variants exhibit consistent trends in response to parameter changes.

Channel Capacity. Our method embeds a 32-bit message per channel in the latent vector. We analyze the impact of increasing the number of channels (N_C), which directly corresponds to the total bit capacity. Table 3 shows that as N_C increases from 1 to 4, the bit capacity increases from 32 to 128. As

Table 3. Ablation study on key parameters for the IPS variant. The results show the impact of channel capacity, axis offsets, and Hermitian symmetry on performance and image quality.

| | N_C | Bits | Axis | PSNR \uparrow | LPIPS \downarrow | <i>Vrf.</i> | <i>Idf.</i> |
|---------------------------|-------|------|--------------|-----------------|--------------------|-------------|-------------|
| Cut-off Imaginary | 1 | 32 | \times | 35.271 | 0.0201 | 0.673 | 0.067 |
| | | | \checkmark | 35.356 | 0.0192 | 0.671 | 0.068 |
| | 2 | 64 | \times | 34.875 | 0.0232 | 0.834 | 0.284 |
| | | | \checkmark | 34.988 | 0.0220 | 0.825 | 0.286 |
| Frequency Restored (Ours) | 3 | 96 | \times | 34.299 | 0.0322 | 0.943 | 0.519 |
| | | | \checkmark | 34.463 | 0.0297 | 0.938 | 0.520 |
| | 4 | 128 | \times | 33.808 | 0.0414 | 0.979 | 0.707 |
| | | | \checkmark | 34.013 | 0.0378 | 0.975 | 0.694 |
| Frequency Restored (Ours) | 1 | 32 | \times | 33.994 | 0.0420 | 0.950 | 0.640 |
| | | | \checkmark | 34.127 | 0.0396 | 0.946 | 0.629 |
| | 2 | 64 | \times | 33.484 | 0.0521 | 0.977 | 0.847 |
| | | | \checkmark | 33.637 | 0.0485 | 0.977 | 0.837 |
| Frequency Restored (Ours) | 3 | 96 | \times | 32.774 | 0.0767 | 0.995 | 0.952 |
| | | | \checkmark | 32.967 | 0.0708 | 0.995 | 0.948 |
| | 4 | 128 | \times | 32.222 | 0.0983 | 0.999 | 0.985 |
| | | | \checkmark | 32.437 | 0.0903 | 0.998 | 0.980 |

expected, this results in a trade-off: detection performance (*Vrf.*, *Idf.*) improves while image quality (PSNR, LPIPS) degrades. A shorter watermark length requires a higher detection threshold to control the false positive rate, which can weaken detection power. We thus determine that the 128-bit setting ($N_C = 4$) is the most suitable, as it ensures stable detection performance.

Hermitian Symmetry for Real-Valued Output. We validate enforcing Hermitian symmetry against naively discarding the imaginary part (Cut-off Imaginary). As shown in Table 3, Hermitian symmetry is crucial for detection, boosting Verification/Identification performance from 0.975/0.694 to 0.998/0.980. The naive approach dilutes the embedded signal, which degrades detection. The paradoxically higher image quality of the naive method simply indicates that the watermark is not embedded correctly. Thus, enforcing symmetry is essential for reliable watermarking.

4. CONCLUSION

In this work, we introduced PhaseMark, a novel post-hoc watermarking framework that achieves state-of-the-art resilience and efficiency without iterative optimization. By directly modulating phase in the latent frequency domain, PhaseMark overcomes the prohibitive computational costs of prior methods, enabling real-time performance while preserving image quality. Our analysis of four variants provides a clear performance-quality trade-off for practical applications. For enhanced security, the watermark payload can be encrypted using cryptographic algorithms like ChaCha20 to ensure confidentiality. PhaseMark presents an efficient new paradigm, paving the way for the large-scale deployment of robust watermarking in the generative AI era.

5. REFERENCES

[1] Robin Rombach, Andreas Blattmann, Dominik Lorenz, Patrick Esser, and Björn Ommer, “High-resolution image synthesis with latent diffusion models,” in *Proceedings of the IEEE/CVF conference on computer vision and pattern recognition*, 2022, pp. 10684–10695.

[2] Ingemar Cox, Matthew Miller, Jeffrey Bloom, Jessica Fridrich, and Ton Kalker, *Digital watermarking and steganography*, Morgan kaufmann, 2007.

[3] Nikos Nikolaidis and Ioannis Pitas, “Copyright protection of images using robust digital signatures,” in *1996 IEEE international conference on acoustics, speech, and signal processing conference proceedings*. IEEE, 1996, vol. 4, pp. 2168–2171.

[4] Lijun Zhang, Xiao Liu, Antoni Martin, Cindy Bearfield, Yuriy Brun, and Hui Guan, “Attack-resilient image watermarking using stable diffusion,” *Advances in Neural Information Processing Systems*, vol. 37, pp. 38480–38507, 2025.

[5] Yiyang Guo, Ruizhe Li, Mude Hui, Hanzhong Guo, Chen Zhang, Chuangjian Cai, Le Wan, et al., “Freqmark: Invisible image watermarking via frequency based optimization in latent space,” *Advances in Neural Information Processing Systems*, vol. 37, pp. 112237–112261, 2024.

[6] Yuxin Wen, John Kirchenbauer, Jonas Geiping, and Tom Goldstein, “Tree-rings watermarks: Invisible fingerprints for diffusion images,” *Advances in Neural Information Processing Systems*, vol. 36, 2024.

[7] Hai Ci, Pei Yang, Yiren Song, and Mike Zheng Shou, “Ringid: Rethinking tree-ring watermarking for enhanced multi-key identification,” *arXiv preprint arXiv:2404.14055*, 2024.

[8] Zijin Yang, Kai Zeng, Kejiang Chen, Han Fang, Weiming Zhang, and Nenghai Yu, “Gaussian shading: Provable performance-lossless image watermarking for diffusion models,” in *Proceedings of the IEEE/CVF Conference on Computer Vision and Pattern Recognition*, 2024, pp. 12162–12171.

[9] Sung Ju Lee and Nam Ik Cho, “Semantic watermarking reinvented: Enhancing robustness and generation quality with fourier integrity,” in *Proceedings of the IEEE/CVF International Conference on Computer Vision*, 2025, pp. 18759–18769.

[10] Tsung-Yi Lin, Michael Maire, Serge Belongie, James Hays, Pietro Perona, Deva Ramanan, Piotr Dollár, and C Lawrence Zitnick, “Microsoft coco: Common objects in context,” in *Computer Vision–ECCV 2014: 13th European Conference, Zurich, Switzerland, September 6–12, 2014, Proceedings, Part V 13*. Springer, 2014, pp. 740–755.

[11] Gustavo Santana, “Gustavosta/stable-diffusion-prompts,” <https://huggingface.co/datasets/Gustavosta/Stable-Diffusion-Prompts>, 2022.

[12] Zijie J Wang, Evan Montoya, David Munechika, Haoyang Yang, Benjamin Hoover, and Duen Horng Chau, “Diffusiondb: A large-scale prompt gallery dataset for text-to-image generative models,” *arXiv preprint arXiv:2210.14896*, 2022.

[13] Kevin Alex Zhang, Lei Xu, Alfredo Cuesta-Infante, and Kalyan Veeramachaneni, “Robust invisible video watermarking with attention,” *arXiv preprint arXiv:1909.01285*, 2019.

[14] Pierre Fernandez, Guillaume Couairon, Hervé Jégou, Matthijs Douze, and Teddy Furon, “The stable signature: Rooting watermarks in latent diffusion models,” in *Proceedings of the IEEE/CVF International Conference on Computer Vision*, 2023, pp. 22466–22477.

[15] Johannes Ballé, David Minnen, Saurabh Singh, Sung Jin Hwang, and Nick Johnston, “Variational image compression with a scale hyperprior,” *arXiv preprint arXiv:1802.01436*, 2018.

[16] Zhengxue Cheng, Heming Sun, Masaru Takeuchi, and Jiro Katto, “Learned image compression with discretized gaussian mixture likelihoods and attention modules,” in *Proceedings of the IEEE/CVF conference on computer vision and pattern recognition*, 2020, pp. 7939–7948.

[17] Xuandong Zhao, Kexun Zhang, Zihao Su, Saastha Vasan, Ilya Grishchenko, Christopher Kruegel, Giovanni Vigna, Yu-Xiang Wang, and Lei Li, “Invisible image watermarks are provably removable using generative ai,” *Advances in Neural Information Processing Systems*, vol. 37, pp. 8643–8672, 2025.

[18] Martin Heusel, Hubert Ramsauer, Thomas Unterthiner, Bernhard Nessler, and Sepp Hochreiter, “Gans trained by a two time-scale update rule converge to a local nash equilibrium,” *Advances in neural information processing systems*, vol. 30, 2017.

[19] Richard Zhang, Phillip Isola, Alexei A Efros, Eli Shechtman, and Oliver Wang, “The unreasonable effectiveness of deep features as a perceptual metric,” in *Proceedings of the IEEE conference on computer vision and pattern recognition*, 2018, pp. 586–595.